Supplement of Atmos. Chem. Phys., 24, 5695–5712, 2024
https://doi.org/10.5194/acp-24-5695-2024-supplement

Atmospheric Chemistry and Physics
Open Access
EGU

Supplement of

Attribution of aerosol particle number size distributions to main sources using an 11-year urban dataset

Máté Vörösmarty et al.

Correspondence to: Máté Vörösmarty (vmate6@student.elte.hu) and Imre Salma (salma.imre@ttk.elte.hu)

Table S1. Start and end dates of the measurement years with the median concentrations of total particle number ($N_{6–1000}$; in 10^3 cm^{-3}), NO, NO_2, O_3, CO, SO_2 and PM_{10} mass (all in μg m^{-3}). The measurements in year Y2 were conducted in the near-city background, whereas the other data were obtained in the urban background of Budapest.

Year	Start	End	$N_{6–1000}$	NO	NO_2	O_3	CO	SO_2	PM_{10}
Y1	3–Nov–2008	2–Nov–2009	11.3	13.4	37	25	547	5.0	33
Y2	19–Jan–2012	18–Jan–2013	4.2	3.9	15.4	51	378	6.1	23
Y3	13–Nov–2013	12–Nov–2014	9.8	19.7	47	18.3	489	4.8	31
Y4	13–Nov–2014	12–Nov–2015	9.4	23	48	20	577	4.6	39
Y5	13–Nov–2015	12–Nov–2016	7.6	17.7	42	25	513	4.8	29
Y6	28–Jan–2017	27–Jan–2018	10.6	20	44	21	534	4.5	28
Y7	28–Jan–2018	27–Jan–2019	10.3	17.2	43	21	669	5.2	36
Y8	28–Jan–2019	27–Jan–2020	10.7	26	42	20	625	4.9	34
Y9	28–Jan–2020	27–Jan–2021	8.6	10.8	33	25	526	5.0	26
Y10	28–Jan–2021	27–Jan–2022	9.6	12.9	36	28	589	4.5	25
Y11	28–Jan–2022	28–Jan–2023	9.0	10.5	31	35	607	5.2	22

Table S2. Seasonal means ± standard deviations of the air temperature (*T*, in °C), relative humidity (RH, in %), wind speed above the rooftop level (WS, in m s^{-1}) and global radiation for individual values > 10 W m^{-2} (GRad, in W m^{-2}) over the whole measurement interval.

Parameter	spring	summer	autumn	winter
T	13.1±6.4	23.4±4.9	13.0±6.4	2.9±4.4
RH	60±19	59±18	75±20	80±16
WS	3.0±1.9	2.7±1.6	2.4±1.6	2.8±1.9
GRad	375±211	442±257	261±145	163±83

Table S3. Final parameters *A* and C_3 after their fine-tuning for the uncertainty estimations of the total particle number concentration ($N_{6–1000}$), particle number concentrations for the diameter channels (in nm) and air pollutants (see Eqs. 2 and 3).

Par.	$N_{6–1000}$	6	7.3	8.9	10.8–451	550	670	816	994	SO_2	NO	NO_2	O_3	CO	PM_{10}
A	1	4	3	2	1	2	3	4	5	4	4	4	4	4	4
C_3	0.1	0.16	0.1	0.1	0.1	0.1	0.1	0.2	0.2	0.15	0.2	0.2	0.15	0.15	0.15

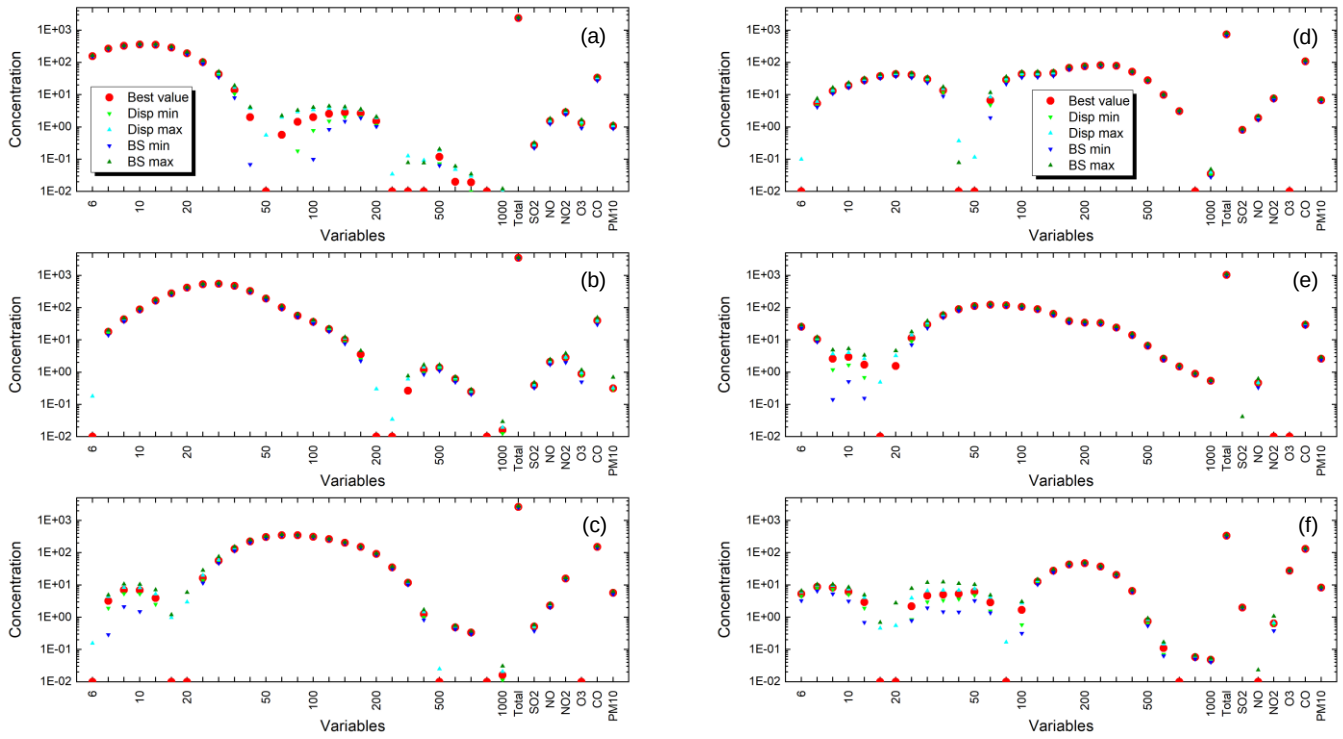

Figure S1. Uncertainty estimations by displacement analysis (Disp) and bootstrapping (BS) in the uncorrected PMF modelling for the sources of nucleation (a), vehicle traffic semi-volatile fraction (b), vehicle traffic solid core fraction (c), diffuse urban (d), secondary inorganic aerosol (e) and ozone-associated aerosol (f) in spring. The concentrations are in cm^{-3} for the particle numbers, and in $\mu g\ m^{-3}$ for air pollutants. The Best values represent the concentration from the base run.

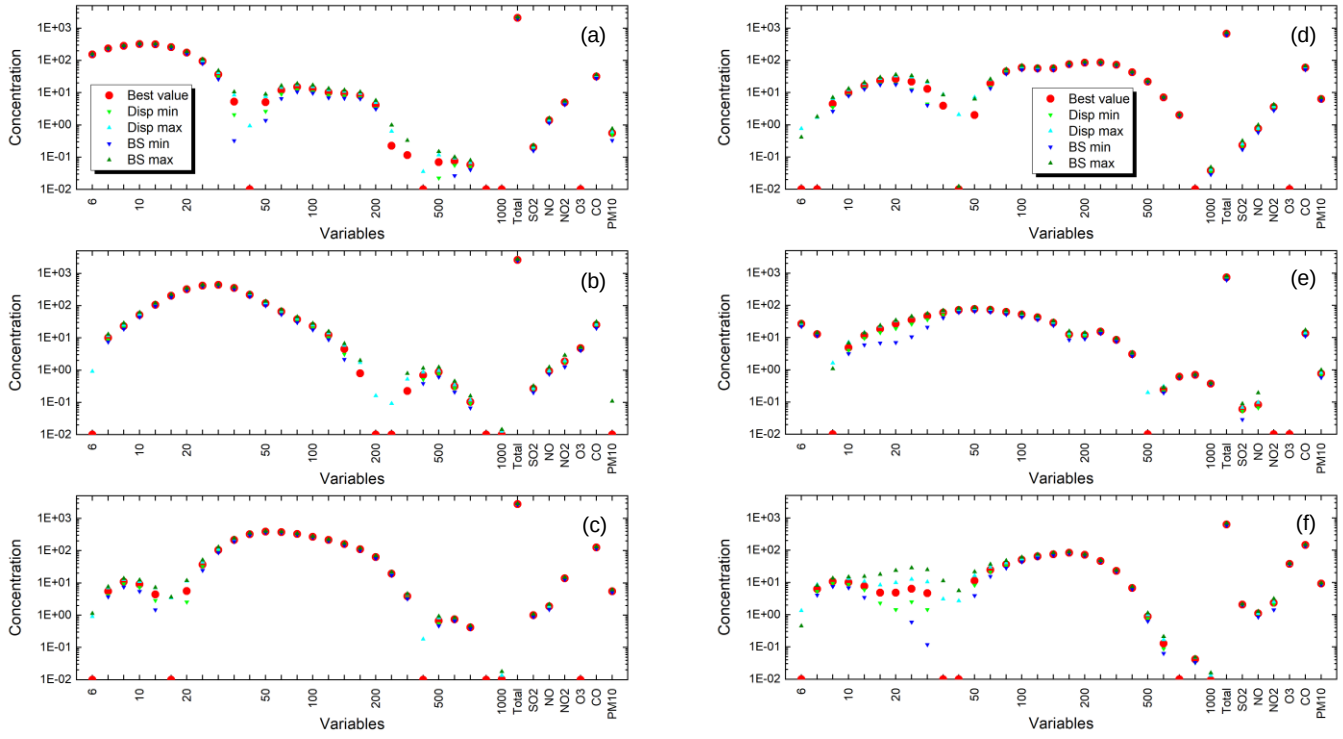

Figure S2. Uncertainty estimations by displacement analysis (Disp) and bootstrapping (BS) in the uncorrected PMF modelling for the sources of nucleation (a), vehicle traffic semi-volatile fraction (b), vehicle traffic solid core fraction (c), diffuse urban (d), secondary inorganic aerosol (e) and ozone-associated aerosol (f) in summer. The concentrations are in cm^{-3} for the particle numbers, and in $\mu g\ m^{-3}$ for air pollutants. The Best values represent the concentration from the base run.

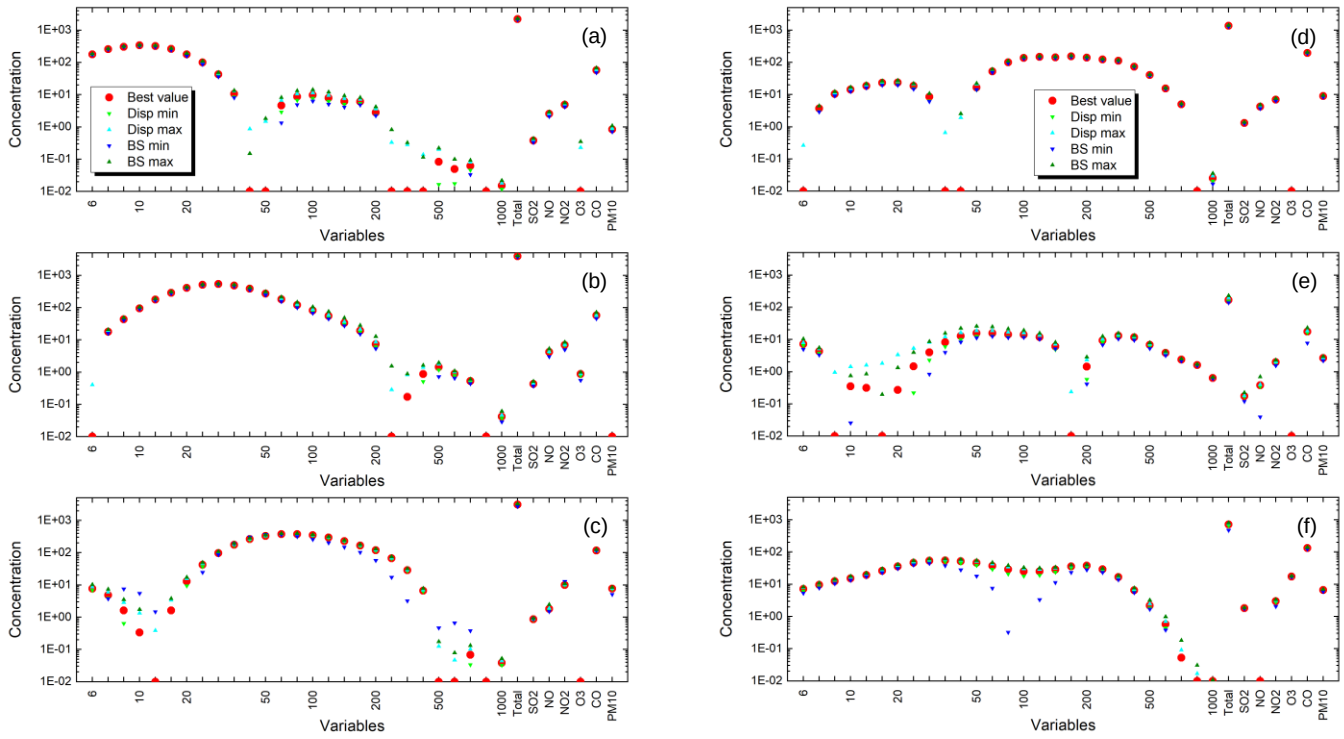

Figure S3. Uncertainty estimations by displacement analysis (Disp) and bootstrapping (BS) in the uncorrected PMF modelling for the sources of nucleation (a), vehicle traffic semi-volatile fraction (b), vehicle traffic solid core fraction (c), diffuse urban (d), secondary inorganic aerosol (e) and ozone-associated aerosol (f) in autumn. The concentrations are in cm^{-3} for the particle numbers, and in $\mu g\ m^{-3}$ for air pollutants. The Best values represent the concentration from the base run.

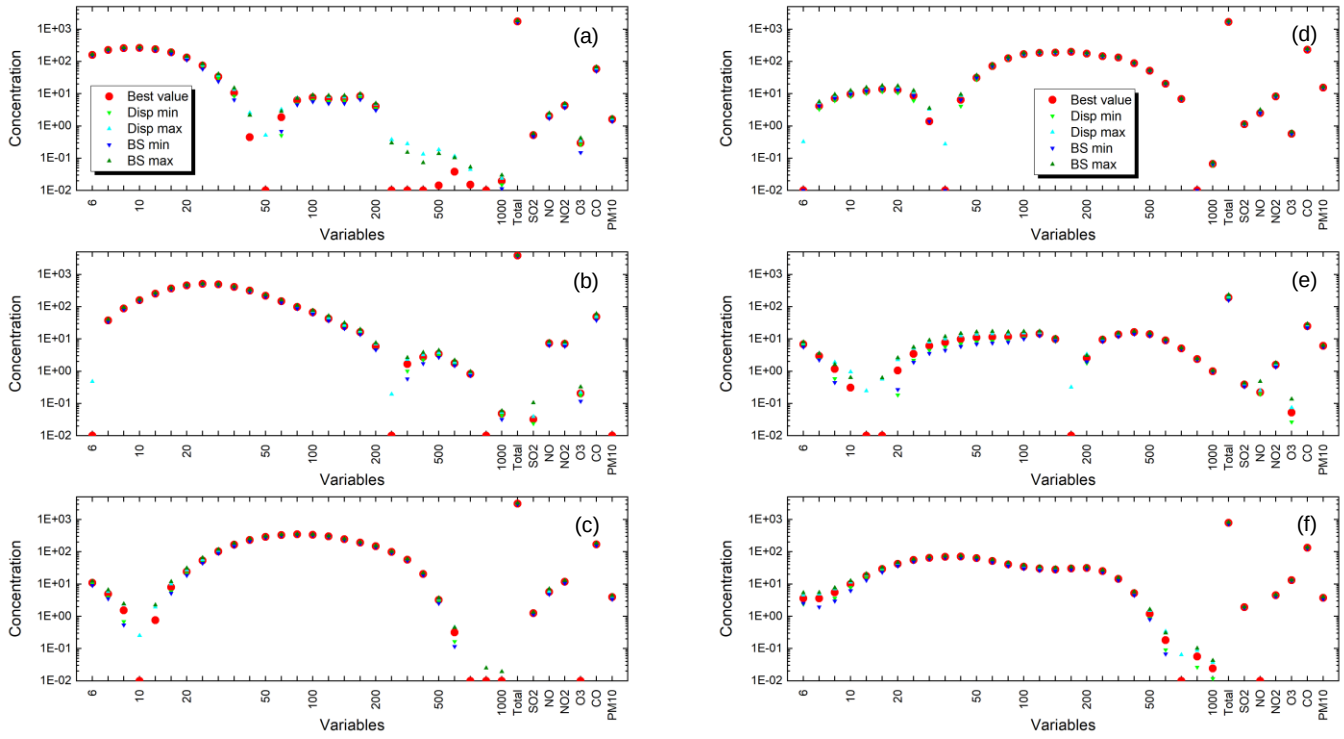

Figure S4. Uncertainty estimations by displacement analysis (Disp) and bootstrapping (BS) in the uncorrected PMF modelling for the sources of nucleation (a), vehicle traffic semi-volatile fraction (b), vehicle traffic solid core fraction (c), diffuse urban (d), secondary inorganic aerosol (e) and ozone-associated aerosol (f) in winter. The concentrations are in cm^{-3} for the particle numbers, and in $\mu g\ m^{-3}$ for air pollutants. The Best values represent the concentration from the base run.

The mean diel variations of the ventilation coefficient ratio and of its MLH and WS constituents exhibited a pattern consisting of a broad band during the daylight period (Fig. S5). The MLH curves showed the maximum value in summer, a lower, but close time series in spring, the minimum value in winter, and a close, but somewhat higher curve in autumn (Fig. S5a). During the evening and night, the curves were similar to each other. The WS time series displayed the largest values in spring, smaller levels in summer and summer and winter, and the smallest values in autumn (Fig. S5b). As a result, the time series of the VC_{ratio} over the peak region were similar to each other in spring and summer, while the ratios in autumn and winter were also similar to each other, but smaller (Fig. S5c). The VC_{ratio} data were above unity (up to 3 in spring and summer) from 07:00 to 16:00 UTC+1, whereas they were < 1 (down to 0.3 in summer) outside this time interval.

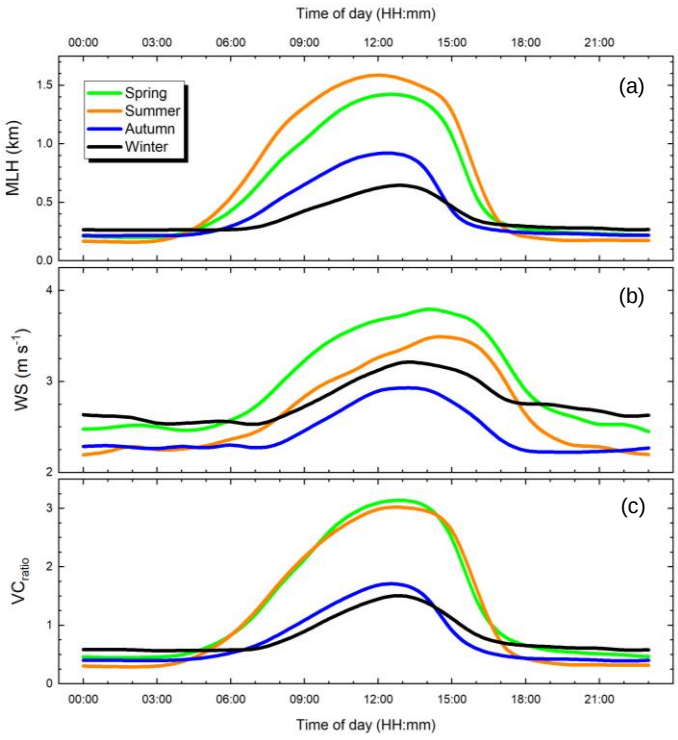

Figure S5. Mean diel variations of the planetary boundary mixing layer height (MLH; a), wind speed (WS; b) and ventilation coefficient ratio (VC_{ratio}; c) separately for spring, summer, autumn and winter.

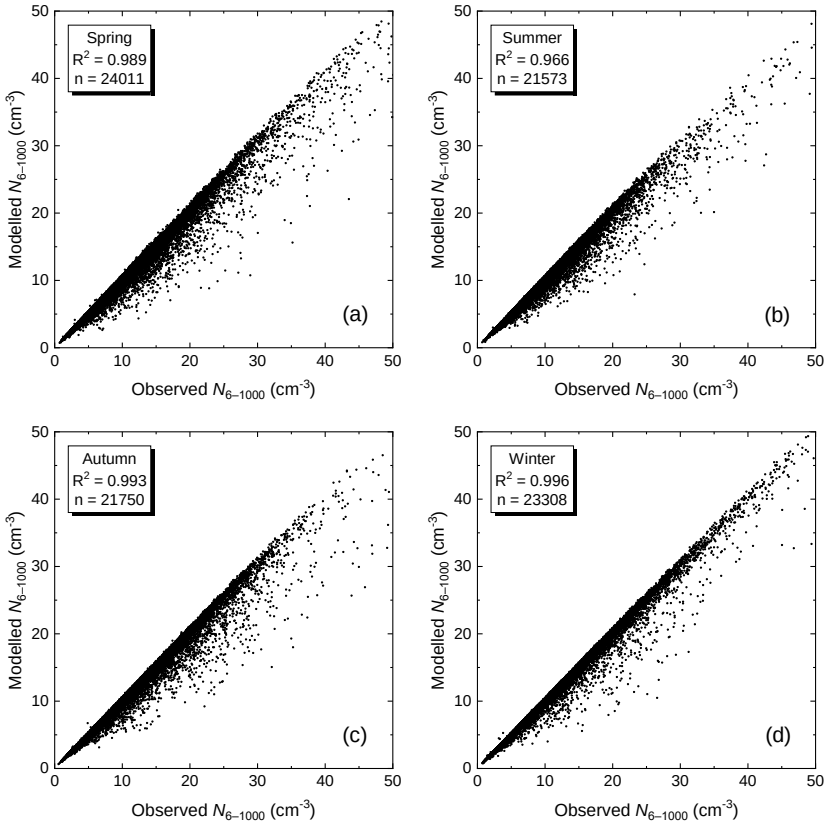

Figure S6. Scatter plots of the modelled (by the uncorrected PMF) and measured total particle number concentrations ($N_{6–1000}$) for spring (a), summer (b), autumn (c) and winter (d). The coefficient of determination (R^2) and total number of observations (n) are also indicated. The seasonal medians of the measured concentrations from spring to winter are 9.2, 8.5, 10.3 and 9.9×10^3 cm^{-3}, respectively.

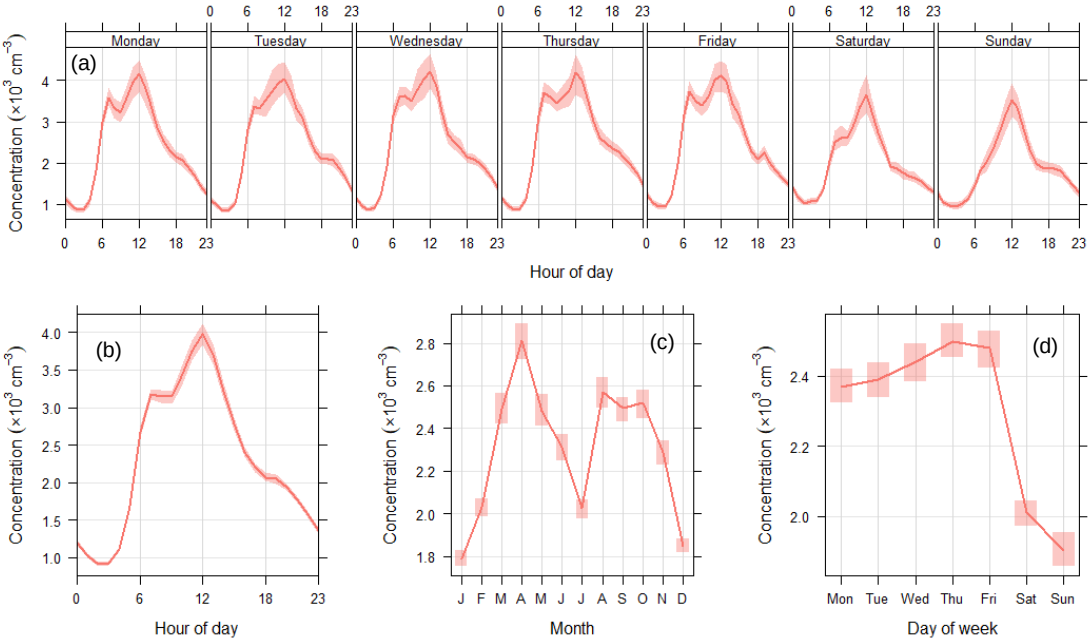

Figure S7. Mean variations of the total particle number concentration associated with the nucleation source in the uncorrected PMF modelling as diel time series for day of week (a), for all days (b), as monthly means for month of year (c) and as daily means for day of week (d). The coloured bands around the lines indicate 95 % confidence interval of the mean.

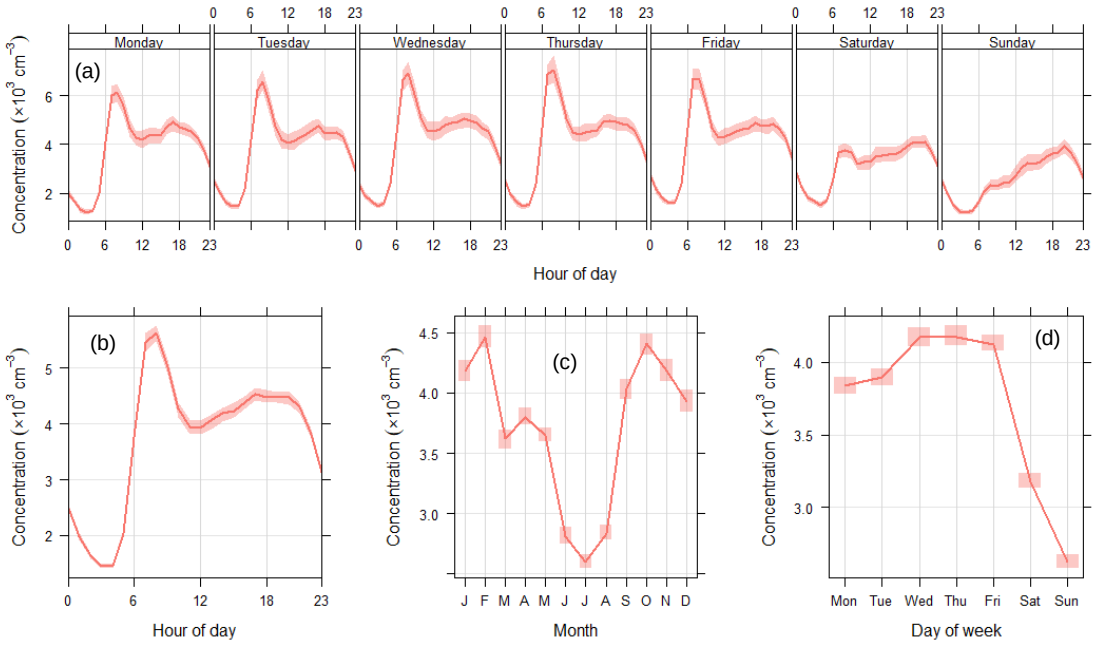

Figure S8. Mean variations of the total particle number concentration associated with the vehicle traffic semi-volatile fraction source in the uncorrected PMF modelling as diel time series for day of week (a), for all days (b), as monthly means for month of year (c) and as daily means for day of week (d). The coloured bands around the lines indicate 95 % confidence interval of the mean.

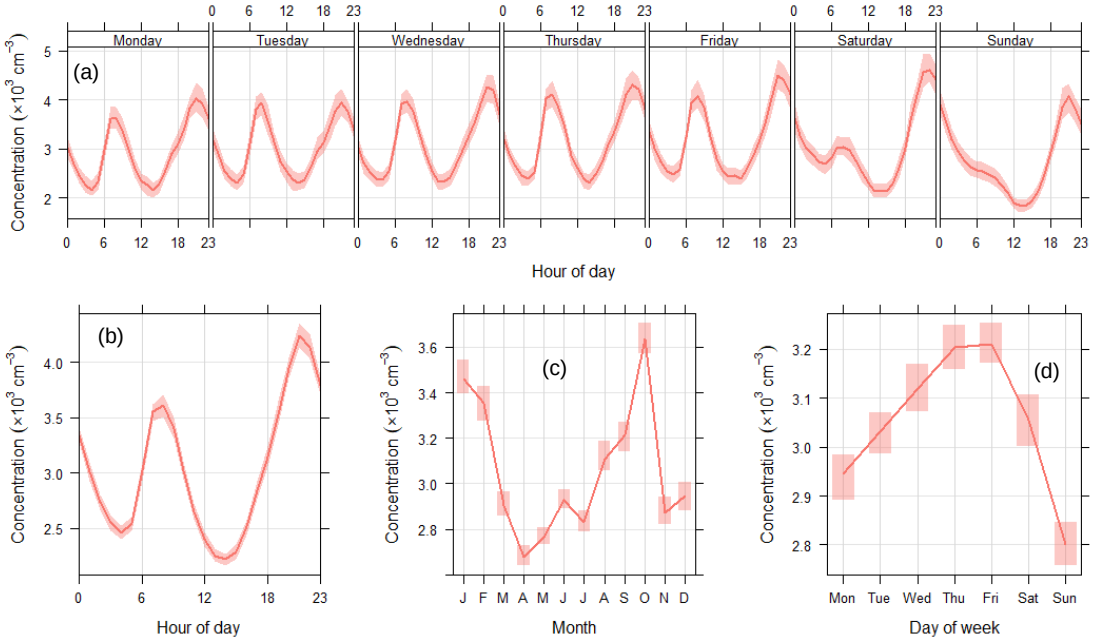

Figure S9. Mean variations of the total particle number concentration associated with the vehicle traffic solid core fraction source in the uncorrected PMF modelling as diel time series for day of week (a), for all days (b), as monthly means for month of year (c) and as daily means for day of week (d). The coloured bands around the lines indicate 95 % confidence interval of the mean.

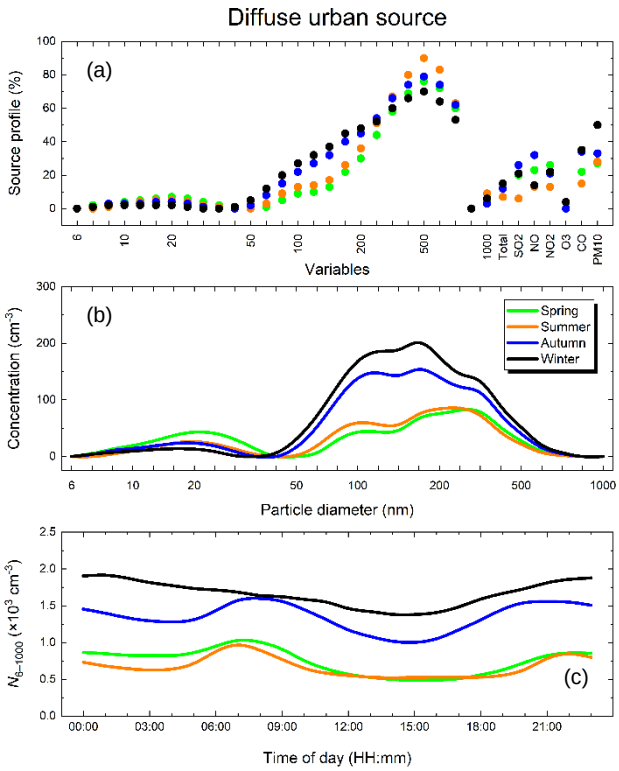

Figure S10. Relative factor profiles (a), factor contributions to the particle number concentrations in the size channels (b), and mean diel variations of the total particle number concentration ($N_{6–1000}$; c) assigned to the urban diffuse source in the uncorrected PMF modelling for spring, summer, autumn and winter. The exact diameters of the size channels are listed in Sect. 2.1.

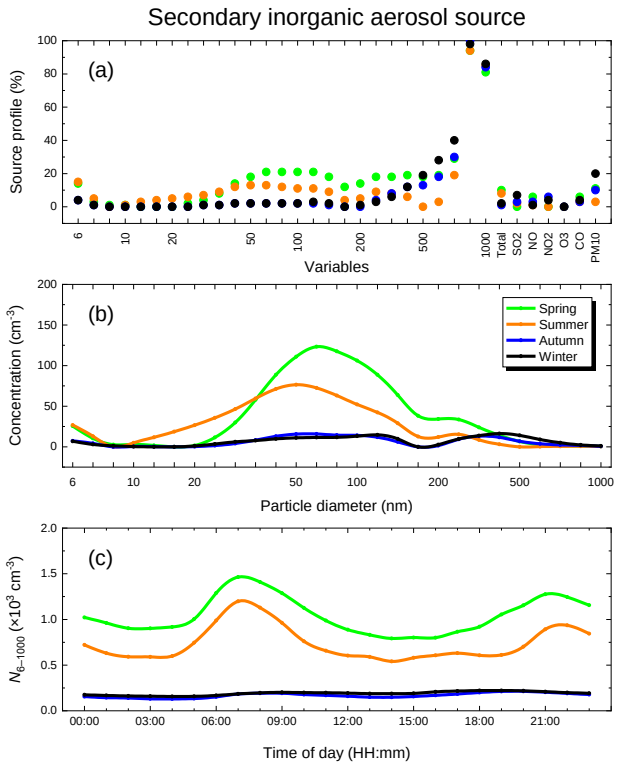

Figure S11. Relative factor profiles (a), factor contributions to the particle number concentrations in the size channels (b), and mean diel variations of the total particle number concentration ($N_{6–1000}$; c) assigned to the source of secondary inorganic aerosol in the uncorrected PMF modelling for spring, summer, autumn and winter. The exact diameters of the size channels are listed in Sect. 2.1.

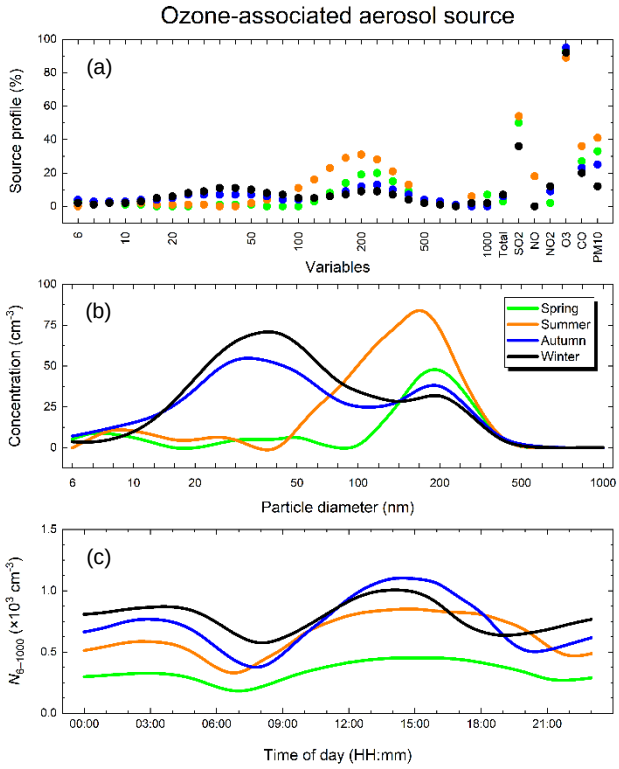

Figure S12. Relative factor profiles (a), factor contributions to the particle number concentrations in the size channels (b), and mean diel variations of the total particle number concentration ($N_{6–1000}$; c) assigned to the O_3-associated secondary aerosol source in the uncorrected PMF modelling for spring, summer, autumn and winter. The exact diameters of the size channels are listed in Sect. 2.1.

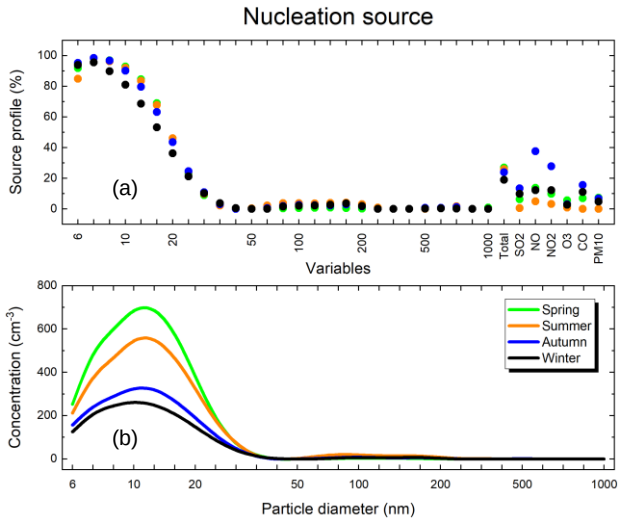

Figure S13. Relative factor profiles (a) and factor contributions to the particle number concentrations in the size channels (b) assigned to the nucleation source in the dispersion-corrected PMF modelling for spring, summer, autumn and winter. The exact diameters of the size channels are listed in Sect. 2.1.

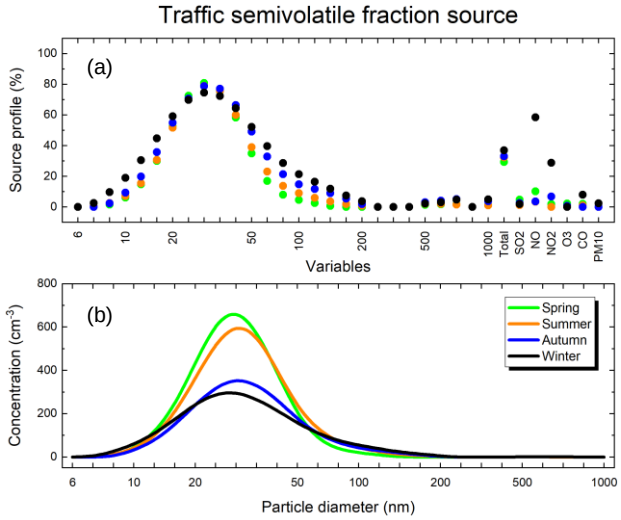

Figure S14. Relative factor profiles (a) and factor contributions to the particle number concentrations in the size channels (b) assigned to the road vehicle traffic semi-volatile fraction source in the dispersion-corrected PMF modelling for spring, summer, autumn and winter. The exact diameters of the size channels are listed in Sect. 2.1.

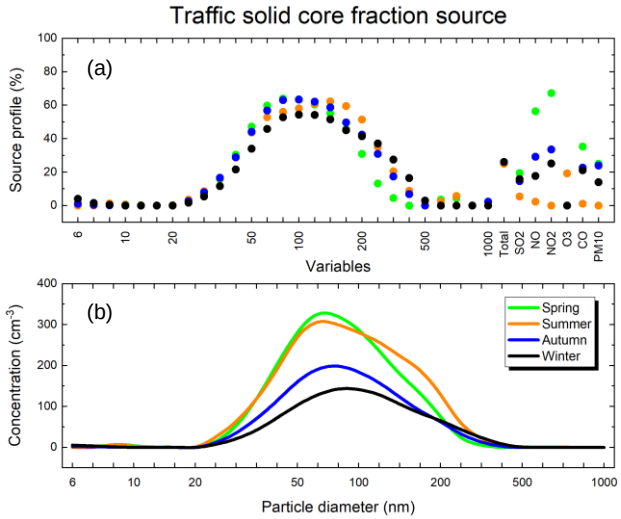

Figure S15. Relative factor profiles (a) and factor contributions to the particle number concentrations in the size channels (b) assigned to road vehicle traffic solid core fraction sources in the dispersion-corrected PMF modelling for spring, summer, autumn and winter. The exact diameters of the size channels are listed in Sect. 2.1.

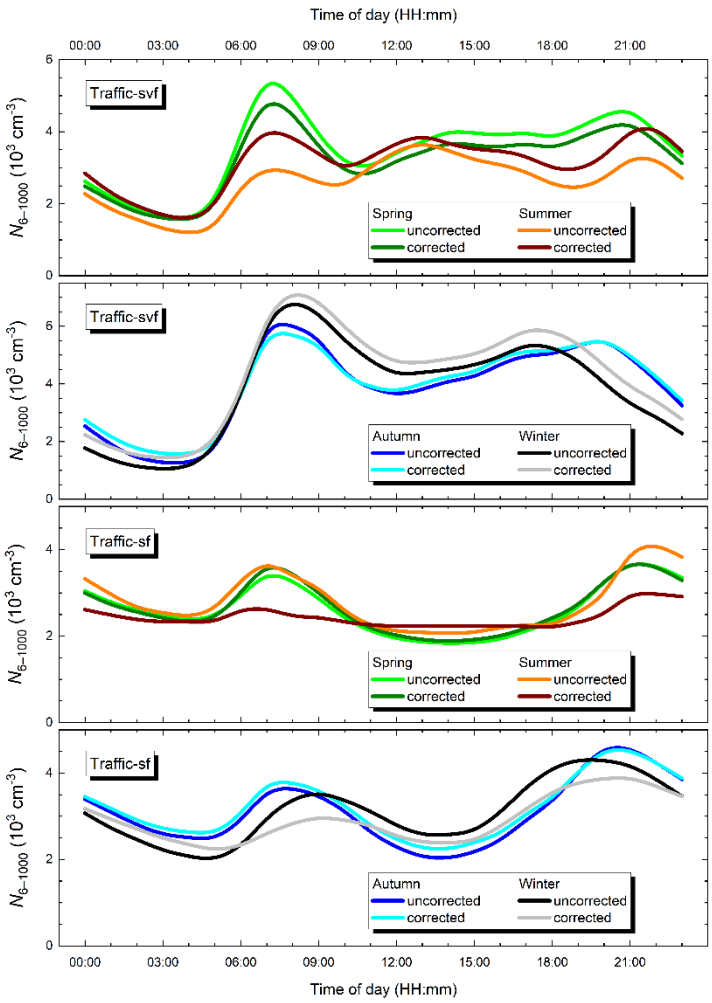

Figure S16. Mean diel variations of the road vehicle traffic semi-volatile fraction (traffic-svf) and road vehicle traffic solid core fraction (traffic-sf) sources derived by the uncorrected PMF and dispersion-corrected PMF models in spring, summer, autumn and winter.

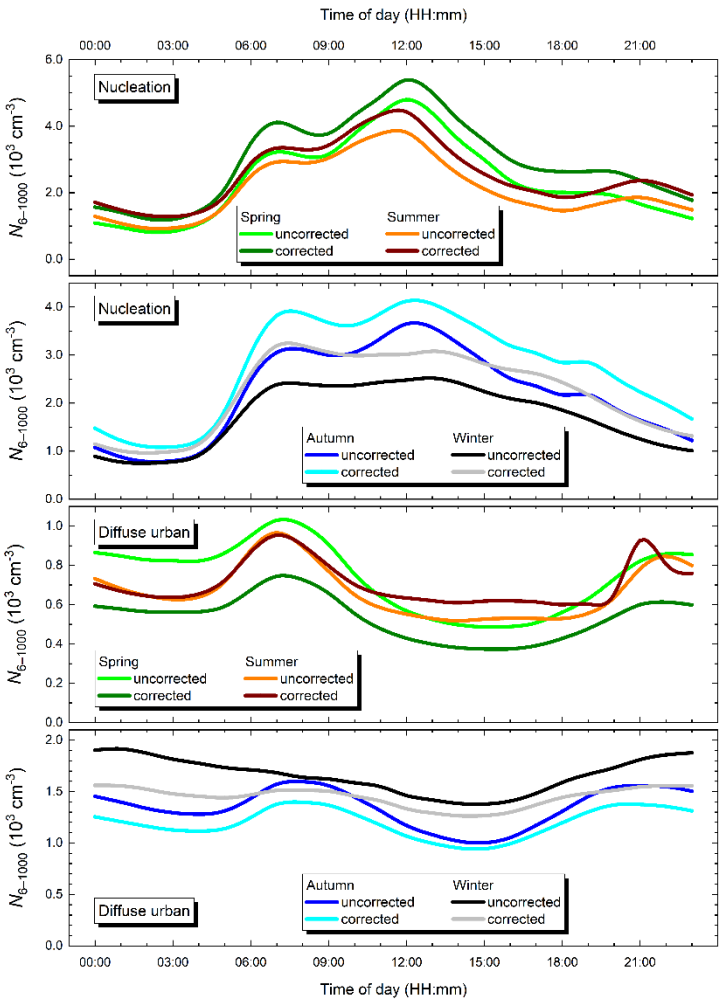

Figure S17. Mean diel variations of the nucleation and diffuse urban sources derived by the uncorrected PMF and dispersion-corrected PMF models in spring, summer, autumn and winter.

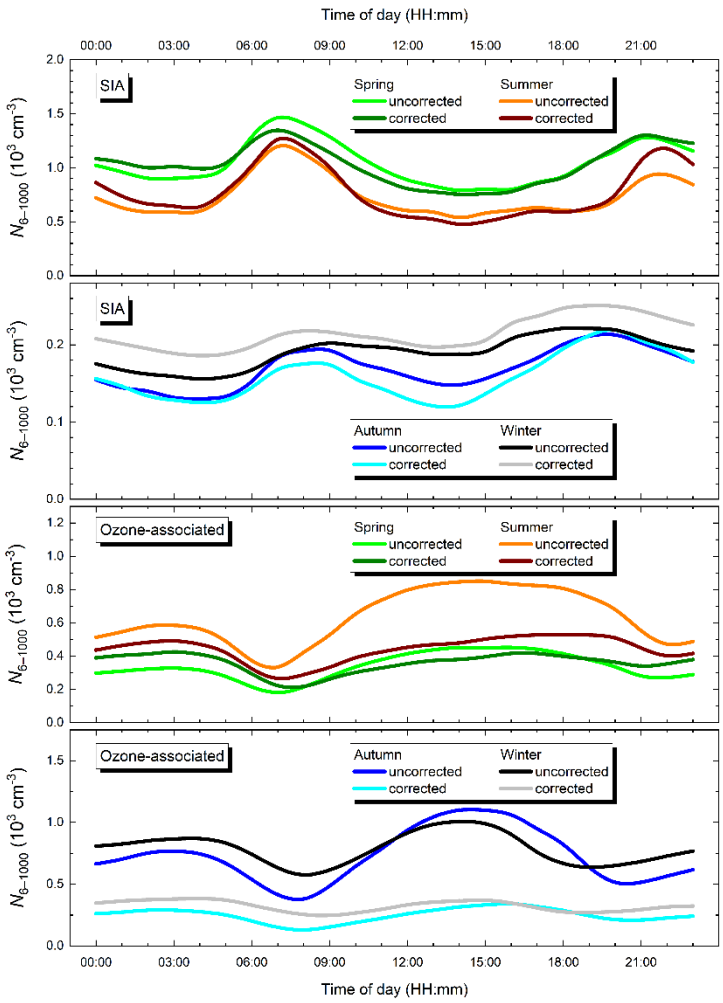

Figure S18. Mean diel variations of sources of the secondary inorganic aerosol (SIA) and ozone-associated secondary aerosol derived by the uncorrected PMF and dispersion-corrected PMF models in spring, summer, autumn and winter.

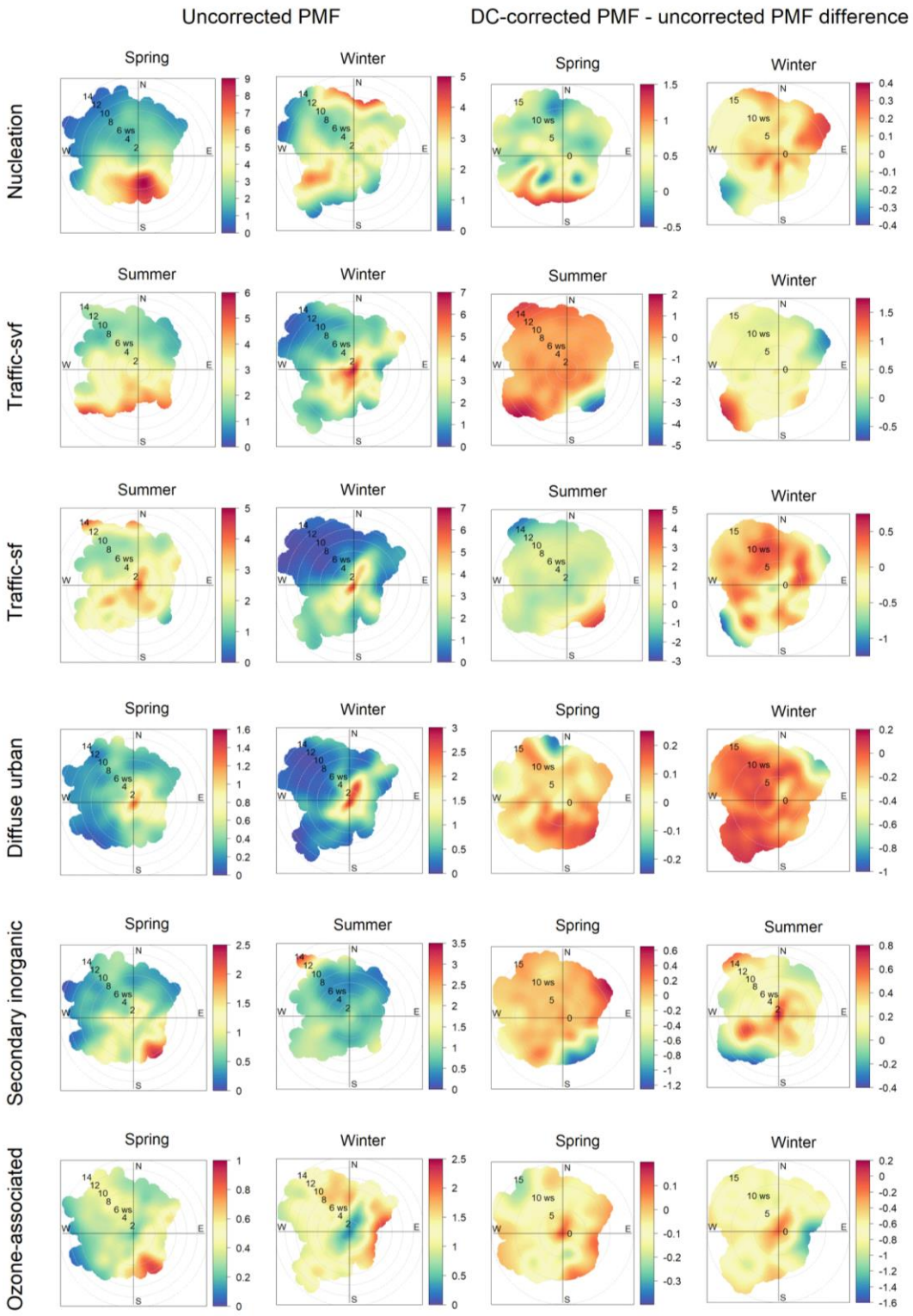

Figure S19. Conditional bivariate probability plots of the contributions to the total particle number concentration ($N_{6–1000}$; in 10^3 cm^{-3}; first and second columns from left) from the nucleation, road vehicle traffic semi-volatile fraction (traffic-svf), road vehicle traffic solid core fraction (traffic-sf), diffuse urban, secondary inorganic aerosol and ozone-associated secondary aerosol sources derived by the uncorrected PMF model, and the (DC-PMF – uncorrected PMF) difference for the $N_{6–1000}$ (in 10^3 cm^{-3}; third and fourth columns from left) in selected season pairs. The values of the WS are given in m s^{-1}. Note the different scales of the colour bar.